



Dissipation instability of Couette-like adiabatic flows in a plane channel

A. Barletta^{a,*}, M. Celli^a, S. Lazzari^b, P.V. Brandão^a

^a Department of Industrial Engineering, Alma Mater Studiorum Università di Bologna, Viale Risorgimento 2, 40136 Bologna, Italy

^b Department of Architecture and Design, University of Genoa, Stradone S. Agostino 37, 16123 Genoa, Italy

ARTICLE INFO

Keywords:

Viscous dissipation
Buoyancy force
Dual flows
Linear stability
Couette flow
Adiabatic walls

ABSTRACT

The mixed convection flow in a plane channel with adiabatic boundaries is examined. The boundaries have an externally prescribed relative velocity defining a Couette-like setup for the flow. A stationary flow regime is maintained with a constant velocity difference between the boundaries, considered as thermally insulated. The effect of viscous dissipation induces a heat source in the flow domain and, hence, a temperature gradient. The nonuniform temperature distribution causes, in turn, a buoyancy force and a combined forced and free flow regime. Dual mixed convection flows occur for a given velocity difference. Their structure is analysed where, in general, only one branch of the dual flows is compatible with the Oberbeck–Boussinesq approximation, for realistic values of the Gebhart number. A linear stability analysis of the basic stationary flows with viscous dissipation is carried out. The stability eigenvalue problem is solved numerically, leading to the determination of the neutral stability curves and the critical values of the Péclet number, for different Gebhart numbers. An analytical asymptotic solution in the special case of perturbations with infinite wavelength is also developed.

1. Introduction

The absence of a transition to hydrodynamic instability, through linear perturbations, for the plane Couette flow is a cornerstone result of fluid mechanics. In fact, early discussions regarding the linear stability of the plane Couette flow date back to papers such as that by Rayleigh [1], while a rigorous proof was provided in more recent times by Romanov [2]. The core assumption of this important achievement is that the fluid is considered isothermal so that no temperature gradient effect may influence the local momentum balance of the fluid. A thorough discussion of the hydrodynamic stability for the plane Couette flow is provided, for instance, in the books by Drazin and Reid [3] and by Schmid and Henningson [4]. Despite the theoretical results of the linear stability analysis, transition to instability and turbulence as a response to finite-amplitude perturbations is observed in several experiments such as those reported by Bottin et al. [5] and by Tillmark and Alfredsson [6]. Transition to instability was indeed proved experimentally for Reynolds numbers around 300.

When a non-isothermal regime is considered, convection heat transfer may cause the linear instability of the plane Couette flow at sufficiently large Rayleigh numbers, where the Rayleigh number is proportional to the temperature difference imposed between the hot lower wall and the cold upper wall [7–9]. The thermal buoyancy force is the cause of the motion by means of an upward heat flux imposed through the temperature boundary conditions. Besides the boundary conditions, a temperature gradient inside the fluid may be caused by the frictional

heating. In fact, a viscous dissipation effect occurs due to the velocity difference between the plane boundaries.

The effect of viscous dissipation may be the unique source of thermal instability in those cases where there is no temperature difference impressed on the fluid by means of the boundary conditions. In fact, the temperature coupling term within the local momentum balance equation can be manifold. The most common coupling terms are the viscous force, since the viscosity depends significantly on the local temperature, and the buoyancy force, since the density depends significantly on the local temperature. The variable viscosity, in connection with viscous dissipation, has been envisaged as a cause of thermally-induced flow instability by Joseph [10,11] and, more recently, by Barletta and Nield [12]. The buoyancy force, as responsible of a viscous dissipation instability, has been also considered in several studies over the last decades [13–18]. Obviously, the physics of the viscous dissipation effect suggests that both the temperature-dependence of the fluid viscosity and the temperature-dependence of the fluid density may contribute in some way to the momentum balance with a relative importance that may vary from case to case. Such a view is virtually compatible with the Oberbeck–Boussinesq model for buoyant flows, as this approximate scheme may include also cases where the viscosity or other fluid properties, such as the thermal diffusivity, undergoes temperature changes [19–21]. The problem is that such an expanded version of the Oberbeck–Boussinesq model is highly complicated by

* Corresponding author.

E-mail address: antonio.barletta@unibo.it (A. Barletta).

a significantly large number of governing parameters. Recently, some early attempts to define the methods for the investigation of flows with a large number of governing parameters have been made, based on machine learning techniques [22]. We are guided by the principle that understanding the basic nature of physical phenomena needs a clear view of appropriate, though simplified, ontologies [23]. For such reasons, the focus of the analysis presented in this paper will be on the classical Oberbeck–Boussinesq approximation. The idea of modelling the fluid viscosity as constant is appropriate as the focus of the Oberbeck–Boussinesq approximation is on convection processes where small temperature changes arise [24–26].

The aim of this paper is bringing a different view on the onset of instability for the Couette flow. Indeed, the term Couette-like flow is more appropriate as we will show that taking into account the effects of viscous dissipation and of the buoyancy force yields a modification of the Couette profile in the stationary basic flow conditions. The arrangement of the Couette boundary conditions specifies adiabatic walls subjected to a velocity difference, where adiabaticity ensures the absence of an external thermal forcing. Non-isothermal flow occurs as a consequence of viscous friction which is, in turn, a consequence of the impressed velocity difference between the boundary walls. This paper is intended as an extension to a Couette-like flow system of the analysis carried out for a Poiseuille-like flow system in a recent study [18]. The analysis of the transition to instability of the basic flow with linear perturbations is carried out under conditions where the viscous dissipation effect is likely to yield major effects, namely the creeping flow of a fluid with a very large Prandtl number [14,18].

The main motivation for the analysis carried out in this paper is the wide area of applications involving a very large Prandtl number and creeping flows. Such applications range from chemical engineering to geophysics. The design of polymeric materials processing and their extrusion, as well as the design of fluid food processing, are typical situations where the viscous dissipation effect may be important [27]. Geophysical systems displaying buoyant flows and natural convection heat transfer with viscous dissipation have been considered by Kincaid and Silver [28] and by van den Berg and Yuen [29]. A model of the excess heat in the upper Earth mantle for the orogenetic evolution explained via the viscous dissipation effect has been developed [28]. Furthermore, natural convection flows in the mantle have been studied by van den Berg and Yuen [29] with a model involving the effects of viscous dissipation, of the internal heating due to radioactive sources and of the adiabatic compression/expansion work. All these applications are relative to extremely viscous fluids with the relatively low velocities typical of creeping flows.

2. Viscous dissipation Buoyant flow

Following the classical Couette-like setup, we consider the Newtonian flow within a plane-parallel channel caused by the relative velocity U_0 between the boundary walls at $z = 0$ and $z = H$. Here, z is the vertical axis perpendicular to the walls and H is the distance between the channel boundaries (see Fig. 1). The width in both the horizontal x and y directions is assumed as infinite. The uniform gravitational acceleration \mathbf{g} is parallel to the z axis, so that $\mathbf{g} = -g \hat{\mathbf{e}}_z$, where $\hat{\mathbf{e}}_z$ is the unit vector of the z axis and g is the modulus of \mathbf{g} .

The boundary conditions prescribed at $z = 0, H$ correspond to impermeable and perfectly adiabatic walls with an imposed relative velocity,

$$\mathbf{u} = 0, \quad \frac{\partial T}{\partial z} = 0 \quad \text{for } z = 0,$$

$$u = U_0 \cos \varphi, \quad v = U_0 \sin \varphi, \quad w = 0, \quad \frac{\partial T}{\partial z} = 0 \quad \text{for } z = H, \quad (1)$$

where $\mathbf{u} = (u, v, w)$ is the velocity field and T is the temperature field, while U_0 is the velocity of the upper boundary wall in the direction defined by the unit vector $(\cos \varphi, \sin \varphi, 0)$, with $0 \leq \varphi \leq \pi/2$.

2.1. Governing equations

Within the framework of the Oberbeck–Boussinesq approximation, the governing equations are given by

$$\nabla \cdot \mathbf{u} = 0, \quad (2a)$$

$$\frac{\partial \mathbf{u}}{\partial t} + (\mathbf{u} \cdot \nabla) \mathbf{u} = -\frac{1}{\rho} \nabla p + g\beta(T - T_0) \hat{\mathbf{e}}_z + \nu \nabla^2 \mathbf{u}, \quad (2b)$$

$$\frac{\partial T}{\partial t} + (\mathbf{u} \cdot \nabla) T = \alpha \nabla^2 T + \frac{\nu}{c} \Phi, \quad (2c)$$

where ρ , β , ν , α and c are the fluid density, thermal expansion coefficient, kinematic viscosity, thermal diffusivity and specific heat of the fluid in the reference thermodynamic state with constant temperature T_0 . In Eqs. (2), t is the time and p is the local difference between the pressure and the hydrostatic pressure. The dissipation function Φ , employed in Eq. (2c) denotes

$$\Phi = \frac{1}{2} \gamma_{ij} \gamma_{ij} \quad \text{using} \quad \gamma_{ij} = \frac{\partial u_i}{\partial x_j} + \frac{\partial u_j}{\partial x_i}, \quad (3)$$

where Einstein's notation for the implicit sum over repeated indices is used, γ_{ij} is the ij Cartesian component of shear rate tensor, while u_i and x_i denote the i th components of the velocity vector \mathbf{u} and of the position vector $\mathbf{x} = (x, y, z)$, respectively.

2.2. Dimensionless formulation

A dimensionless formulation of Eqs. (1) and (2) can be achieved by the scaling

$$\frac{\mathbf{x}}{H} = \frac{(x, y, z)}{H} \rightarrow (x, y, z) = \mathbf{x}, \quad \frac{t}{H^2/\alpha} \rightarrow t,$$

$$\frac{\mathbf{u}}{\alpha/H} = \frac{(u, v, w)}{\alpha/H} \rightarrow (u, v, w) = \mathbf{u}, \quad \frac{p}{\rho\alpha\nu/H^2} \rightarrow p,$$

$$\frac{T - T_0}{\Delta T} \rightarrow T, \quad \frac{\Phi}{\alpha^2/H^4} \rightarrow \Phi \quad \text{using} \quad \Delta T = \frac{\alpha\nu}{g\beta H^3}. \quad (4)$$

By employing Eq. (4), one can rewrite Eqs. (2) in a dimensionless form, namely

$$\nabla \cdot \mathbf{u} = 0, \quad (5a)$$

$$\frac{1}{\text{Pr}} \left[\frac{\partial \mathbf{u}}{\partial t} + (\mathbf{u} \cdot \nabla) \mathbf{u} \right] = -\nabla p + T \hat{\mathbf{e}}_z + \nabla^2 \mathbf{u}, \quad (5b)$$

$$\frac{\partial T}{\partial t} + (\mathbf{u} \cdot \nabla) T = \nabla^2 T + \text{Ge} \Phi, \quad (5c)$$

while the dimensionless boundary conditions (1) are given by

$$\mathbf{u} = 0, \quad \frac{\partial T}{\partial z} = 0 \quad \text{for } z = 0,$$

$$u = \text{Pe} \cos \varphi, \quad v = \text{Pe} \sin \varphi, \quad w = 0, \quad \frac{\partial T}{\partial z} = 0 \quad \text{for } z = 1. \quad (6)$$

In Eqs. (5b), (5c) and (6), the Prandtl number, Pr, the Gebhart number, Ge, and the Péclet number, Pe, are defined as

$$\text{Pr} = \frac{\nu}{\alpha}, \quad \text{Ge} = \frac{g\beta H}{c}, \quad \text{Pe} = \frac{U_0 H}{\alpha}. \quad (7)$$

3. Dual adiabatic flows

Fully developed, parallel and stationary flows satisfying Eqs. (5) and (6) do exist with a horizontal velocity field $(u_b, v_b, 0)$ which depends just on the vertical coordinate z . We introduced the subscript b meant to indicate the “basic solution”. With these specifications, Eq. (5a) is identically satisfied, while Eqs. (5b) and (5c) are simplified to

$$-\frac{\partial p_b}{\partial x} + \frac{d^2 u_b}{dz^2} = 0, \quad (8a)$$

$$-\frac{\partial p_b}{\partial y} + \frac{d^2 v_b}{dz^2} = 0, \quad (8b)$$

$$-\frac{\partial p_b}{\partial z} + T_b = 0, \quad (8c)$$

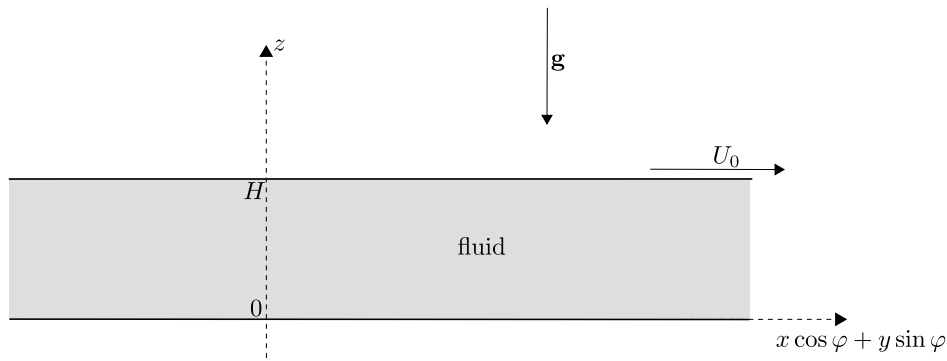


Fig. 1. A sketch of the flow system.

$$u_b \frac{\partial T_b}{\partial x} + v_b \frac{\partial T_b}{\partial y} = \nabla^2 T_b + \text{Ge} \left[\left(\frac{du_b}{dz} \right)^2 + \left(\frac{dv_b}{dz} \right)^2 \right]. \quad (8d)$$

Starting from the formulation of the boundary conditions (6), we have defined an inclination angle φ between the upper wall velocity direction and the x axis, so that the basic velocity $(u_b, v_b, 0)$ is everywhere proportional to the unit vector $(\cos \varphi, \sin \varphi, 0)$. If $\varphi = 0$, the basic velocity is parallel to the x axis, while with $\varphi = \pi/2$ the basic velocity is oriented along the y axis. Oblique flows correspond to generic angles $0 < \varphi < \pi/2$. We emphasise that the Couette-like nature of these flows is not influenced by the choice of φ . In fact, whatever is the angle φ , the velocity distribution is parallel to a horizontal axis defined by the unit vector $(\cos \varphi, \sin \varphi, 0)$. Whether this axis coincides with the x axis or the y axis does not alter the physics. The reason for introducing this apparently useless complication with respect to the traditional descriptions of the Couette flow, is due to our commitment to develop a linear stability analysis of the basic flows. As it will become clearer later on, the linear stability analysis requires consideration of every possible horizontal orientations of the wave vector associated with the perturbation mode. One can equivalently decide to consider an inclined basic velocity and a wave vector parallel to the x axis or a basic velocity parallel to the x axis and an inclined wave vector. We will follow the former scheme. For a formal proof of the mentioned equivalence between the two schemes, we refer the reader to [Appendix](#).

It is easily verified that the basic solution satisfying Eqs. (8) and the boundary conditions (6) is given by

$$\begin{aligned} u_b &= \text{Pe} F(z) \cos \varphi, & v_b &= \text{Pe} F(z) \sin \varphi, \\ T_b &= \text{Pe} A (x \cos \varphi + y \sin \varphi) + \text{Pe}^2 G(z), \\ \nabla p_b &= \left(\text{Pe} F''(z) \cos \varphi, \text{Pe} F''(z) \sin \varphi, T_b \right). \end{aligned} \quad (9)$$

Here, primes are used for the derivatives with respect to z . Equations (6) and (8) are satisfied provided that functions $F(z)$ and $G(z)$ are the polynomials

$$\begin{aligned} F(z) &= z + \frac{A}{12} z(z-1)(2z-1), \\ G(z) &= \frac{z^2}{1440} \{ 2Az [A(6z^2 - 15z + 10) + 120] \\ &\quad - \text{Ge} [A^2(12z^4 - 36z^3 + 40z^2 - 20z + 5) + 120A(z-1)^2 + 720] \}, \end{aligned} \quad (10)$$

while the constant A is equal either to A_- or to A_+ , defined as

$$A_- = 12 \frac{15 - \sqrt{5(45 - \text{Ge}^2)}}{\text{Ge}}, \quad A_+ = 12 \frac{15 + \sqrt{5(45 - \text{Ge}^2)}}{\text{Ge}}. \quad (11)$$

It is easily verified that $F'''(z) = A$. This result implies that the basic temperature gradient in the horizontal x and y directions is independent of z . Eqs. (9)–(11) describe horizontal flows where the velocity field is inclined an angle φ to the x axis. In fact, Eq. (10) yields

$$\int_0^1 F(z) dz = \frac{1}{2}, \quad (12)$$

which means that the average dimensionless velocity in the flow direction is equal to $\text{Pe}/2$, which is the mean velocity of the boundary walls. In other words, in the reference frame where the mean velocity of the boundary walls is zero, the average velocity of the fluid is zero and, hence, also the flow rate is zero. In the absence of viscous dissipation, such a constraint is characteristic of the Couette flow.

On account of Eq. (11), we may have $A = A_-$ or $A = A_+$. As a consequence, Eqs. (9) and (10) entail the existence of dual flows corresponding to the same prescribed values of Pe and Ge . These dual flows are allowed only with $\text{Ge} \leq 3\sqrt{5} \approx 6.70820$. With $\text{Ge} = 3\sqrt{5}$, $A_- = A_+$ and the dual flows coincide. It must be mentioned that this maximum Gebhart number is an extremely large value for any real-world system.

By employing Eq. (9), one can infer that function $F(z)$ yields the basic velocity profile with the Péclet number being an overall constant factor. Similarly, with the feature $G(0) = 0$ displayed by Eq. (10), the function $G(z)$ yields (up to an overall factor Pe^2) the temperature difference between a given position z and the bottom boundary, $z = 0$, in the basic state for fixed x and y . With these considerations in mind, one may view the plots of $F(z)$ and $G(z)$ as representations of the velocity and temperature distributions on a transverse, $x \cos \varphi + y \sin \varphi = \text{constant}$, cross-section of the channel. An interesting characteristic is that both $F(z)$ and $G(z)$ depend on a single parameter, Ge .

Figs. 2 and 3 show some plots of $F(z)$ and $G(z)$ with different Gebhart numbers, relative to either the A_- branch or the A_+ branch. The flow conditions in the two solution branches are utterly different either with respect to the velocity or to the temperature profiles. Fig. 2, relative to the A_- branch, displays just slight changes from the linear velocity profile of the isothermal Couette flow. Values such as $\text{Ge} = 1$ or 2 are very large for most applications except for geophysical or astrophysical systems. The influence of an increasing Gebhart number in the A_- branch is more marked for the temperature profiles $G(z)$. Fig. 3 shows a much more significant influence of the Gebhart number on examining the velocity and temperature profiles for the A_+ branch. Here, the similarity to the Couette linear profile is almost absent for all the considered Gebhart numbers. Such velocity profiles describe a bidirectional flow with $F(z)$ changing from positive to negative across the channel cross-section.

We mention that taking $\text{Ge} = 0$ means switching off the effect of viscous dissipation as it comes out from Eq. (5c). This limiting case yields a linear Couette velocity profile with a uniform temperature distribution as displayed by the black lines in Fig. 2. With regard to the behaviour for small Gebhart numbers, the A_- branch shows the asymptotic expressions

$$\begin{aligned} A &= A_- = 2 \text{Ge} + \mathcal{O}(\text{Ge}^3), \\ F(z) &= z + \frac{\text{Ge}}{6} z(z-1)(2z-1) + \mathcal{O}(\text{Ge}^3), \end{aligned}$$

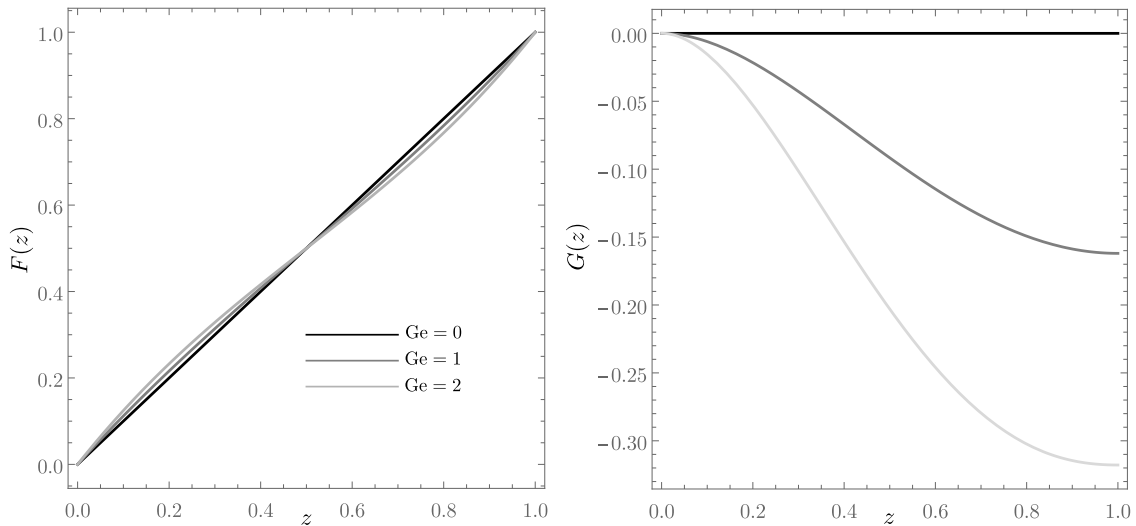


Fig. 2. Plots of $F(z)$ and $G(z)$ for the $A = A_-$ branch with different values of Ge .

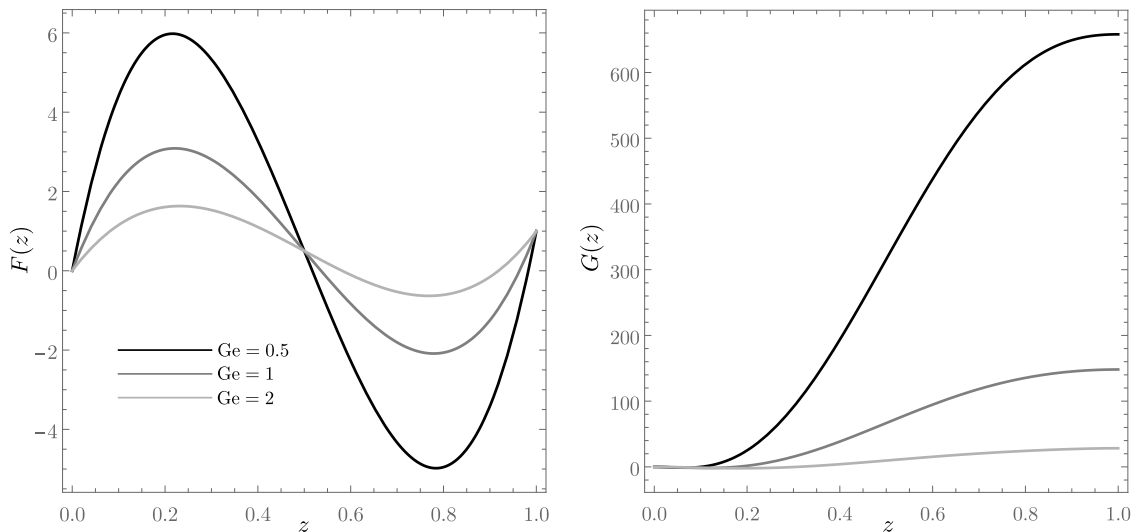


Fig. 3. Plots of $F(z)$ and $G(z)$ for the $A = A_+$ branch with different values of Ge .

$$G(z) = \frac{Ge}{6} z^2 (2z - 3) + \frac{Ge^2}{180} z^2 [z (6z^2 - 45z + 70) - 30] + \mathcal{O}(Ge^3). \tag{13}$$

A direct consequence of Eqs. (9) and (13) is that the A_- branch solution attained with $Ge \rightarrow 0$ yields the isothermal Couette flow,

$$u_b = Pe z \cos \varphi, \quad v_b = Pe z \sin \varphi, \quad w_b = 0, \quad T_b = 0, \quad \nabla p_b = 0. \tag{14}$$

On the contrary, the A_+ branch displays a singular behaviour in the limit $Ge \rightarrow 0$. In fact,

$$A = A_+ = \frac{360}{Ge} - 2Ge + \mathcal{O}(Ge^3),$$

$$F(z) = \frac{30 z (z - 1)(2z - 1)}{Ge} + z - \frac{Ge}{6} z (z - 1)(2z - 1) + \mathcal{O}(Ge^3),$$

$$G(z) = \frac{180 z^3 (6z^2 - 15z + 10)}{Ge^2} - \frac{30 z^2 (36z^4 - 108z^3 + 120z^2 - 62z + 15)}{Ge} - 2 z^2 (6z^3 - 20z + 15) + \frac{Ge z^2}{6} (72z^4 - 216z^3 + 240z^2 - 122z + 27) - \frac{Ge^2 z^2}{180} (6z^3 - 45z^2 + 70z - 30) + \mathcal{O}(Ge^3). \tag{15}$$

Eq. (15) shows that the A_+ solution branch blows up when $Ge \rightarrow 0$. In other words, we reach the reasonable conclusion that, by switching off the effect of viscous dissipation or, equivalently, by setting $Ge = 0$, there is a unique possible solution: the isothermal Couette flow (14). The singular behaviour of the A_+ branch entails an extremely marked influence of small values of Ge on the velocity and temperature gradients in the z direction. For instance, by lowering Ge from 10^{-3} to 10^{-6} , one gets an amplification of the maximum temperature difference across the range $0 \leq z \leq 1$ of one million times. We mention that such small values of Ge are not unlikely in laboratory experiments. This scenario is quite similar to that discussed in Barletta et al. [30] with reference to Poiseuille-like adiabatic flows with viscous dissipation in an adiabatic channel. Following that discussion, we share the same conclusion: the A_+ solution branch is incompatible with the assumptions behind the Oberbeck–Boussinesq approximation except for extremely large values of Ge . Therefore, exactly as in the analysis presented by Barletta et al. [18], our investigation of linear instability will be focussed on the A_- branch.

For the sake of completeness, Fig. 4 provides an illustration of what happens when Ge is close to its maximum value allowed for the existence of the basic solution (9)–(11), i.e. $Ge = 3\sqrt{5}$. If the two branches, A_- and A_+ , coincide at the maximum Gebhart number,

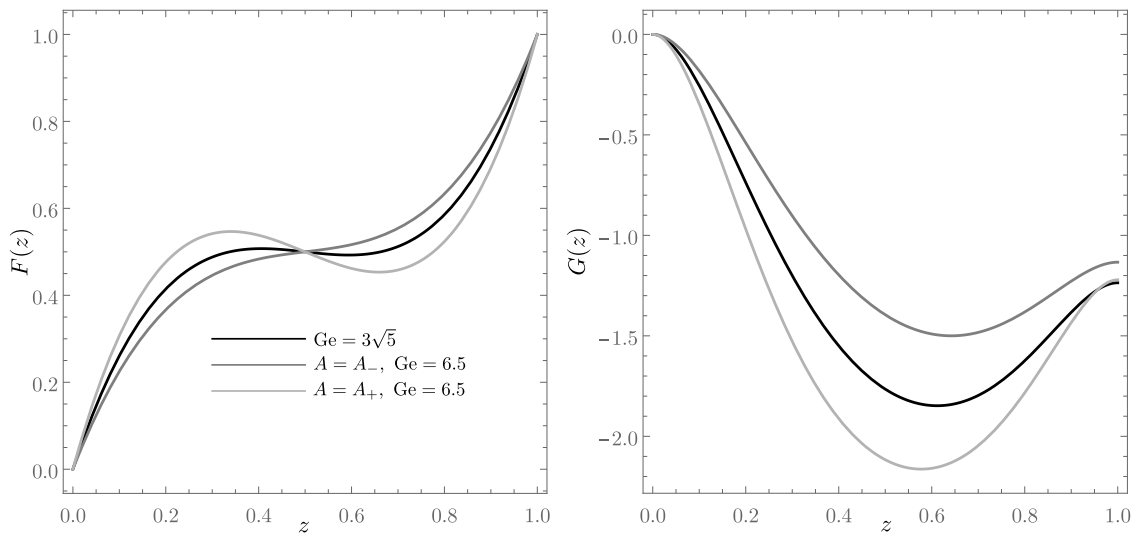


Fig. 4. Plots of $F(z)$ and $G(z)$ for the $A = A_-$ branch and the $A = A_+$ branch with an extremely large value of Ge close to the maximum, $Ge = 3\sqrt{5}$.

they become very similar both for the velocity profile and for the temperature profile when Ge is slightly smaller than the maximum.

4. Onset of the instability

The discussion provided in Section 3 drove the focus of this study to the branch A_- . The features of this branch, as gathered analytically from Eqs. (9)–(11) and graphically from Fig. 2, include a Couette-like shape of the velocity profile, with small departures from the linear trend, and a wide vertical range where $\partial T_b/\partial z < 0$. The latter feature suggests a potential thermal instability of the flow. If and when such potentially unstable temperature distribution actually leads to the onset of a convective instability is the aim of the forthcoming investigation.

4.1. Small-amplitude perturbations

According to the usual modal analysis of the linear instability, we perturb the basic state with small-amplitude wavelike disturbances

$$\begin{pmatrix} \mathbf{u} \\ p \\ T \end{pmatrix} = \begin{pmatrix} \mathbf{u}_b \\ p_b \\ T_b \end{pmatrix} + \varepsilon \begin{pmatrix} \mathbf{U}(z) \\ P(z) \\ \Theta(z) \end{pmatrix} e^{ikx} e^{\lambda t}, \quad (16)$$

where $\varepsilon \ll 1$ is a small positive perturbation parameter, k is the wavenumber and λ is a complex parameter. The real part of such a complex variable, λ_r , yields the temporal growth rate while its imaginary part is $-\omega$, where ω is the angular frequency of the wave. The physical meaning of λ_r arises when the stable or unstable behaviour of the disturbance must be assessed. The linear instability occurs when $\lambda_r > 0$, while $\lambda_r = 0$ defines the neutral stability condition. The neutral stability is the parametric threshold condition for the onset of the instability.

We note that Eq. (16) defines plane wave disturbances travelling along the horizontal x direction. There is no lack of generality in this assumption as the basic flow direction is parallel to the $x \cos \varphi + y \sin \varphi$ axis, with an arbitrary angle φ within the range $0 \leq \varphi \leq \pi/2$. Hence, the x direction is arbitrary, relatively to the direction of the basic flow. By varying the angle, one can span all possible oblique modes of perturbation ranging from $\varphi = 0$, for the transverse modes, to $\varphi = \pi/2$, for the longitudinal modes. The Cartesian components of $\mathbf{U}(z)$ are denoted as $U(z)$, $V(z)$ and $W(z)$. By employing the basic solution, Eqs. (9) and (10), and by substituting Eq. (16) into Eqs. (5) and (6), we obtain

$$W' + ikU = 0, \quad (17a)$$

$$\frac{1}{Pr} [\lambda U + ik Pe F(z) U \cos \varphi + Pe F'(z) W \cos \varphi]$$

$$= -ikP + U'' - k^2 U, \quad (17b)$$

$$\frac{1}{Pr} [\lambda V + ik Pe F(z) V \cos \varphi + Pe F'(z) W \sin \varphi] = V'' - k^2 V, \quad (17c)$$

$$\frac{1}{Pr} [\lambda W + ik Pe F(z) W \cos \varphi] = -P' + \Theta + W'' - k^2 W, \quad (17d)$$

$$\lambda \Theta + ik Pe F(z) \Theta \cos \varphi + Pe A (U \cos \varphi + V \sin \varphi) + Pe^2 G'(z) W = \Theta'' - k^2 \Theta + 2 Ge Pe F'(z) [(U' + ik W) \cos \varphi + V' \sin \varphi], \quad (17e)$$

with the boundary conditions

$$U = 0, \quad \Theta' = 0 \quad \text{for } z = 0, 1. \quad (18)$$

4.2. Creeping flow

Eqs. (17) and (18) yield a system of homogeneous ordinary differential equations with homogeneous boundary conditions, i.e., the stability eigenvalue problem. A reasonable approximation is the assumption that the Prandtl number of the fluid is very large so that the dynamics of the perturbations is that of a creeping buoyant flow [18]. In fact, a very large Prandtl number identifies a very viscous fluid with a small thermal diffusivity. Both these features, large viscosity and small thermal diffusivity, are present when the flow internal heating due to viscous dissipation is significant.

Mathematically, one takes the limit $Pr \rightarrow \infty$ with $Pe \sim \mathcal{O}(1)$ in Eqs. (17b)–(17d). Thus, Eq. (17c) simplifies to $V'' - k^2 V = 0$. Since Eq. (18) prescribes $V = 0$ at $z = 0, 1$, the only possible solution is $V(z) = 0$ for every z . Owing to the relation linking U and W' , Eq. (17a), one can rearrange Eqs. (17b), (17d) and (17e) in order to attain a reformulation of the stability eigenvalue problem using only the eigenfunctions W and Θ , namely

$$W'''' - 2k^2 W'' + k^4 W - k^2 \Theta = 0, \quad (19a)$$

$$\Theta'' - [k^2 + \lambda + ik Pe F(z) \cos \varphi] \Theta + \frac{2i Ge Pe F'(z) \cos \varphi}{k} (W'' + k^2 W) - \frac{i Pe A \cos \varphi}{k} W' - Pe^2 G'(z) W = 0, \quad (19b)$$

$$W = 0, \quad W' = 0, \quad \Theta' = 0 \quad \text{for } z = 0, 1. \quad (19c)$$

With the aim of determining the neutral stability condition, the real part of λ is set to zero so that $\lambda = -i\omega$.

4.3. Infinite wavelength perturbations

An asymptotic solution of Eqs. (19) can be sought for very small wavenumbers. A convenient reformulation of Eqs. (19) is obtained by

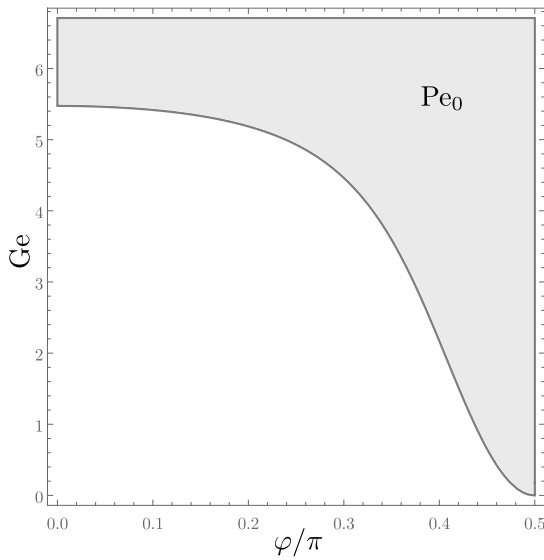


Fig. 5. Domain of existence (grey region) of a neutral stability condition, $Pe = Pe_0$, with $A = A_-$ and $k \rightarrow 0$.

defining

$$\hat{\theta} = k \theta, \tag{20}$$

so that one may write

$$W'''' - 2k^2 W'' + k^4 W - k \hat{\theta} = 0, \tag{21a}$$

$$\hat{\theta}'' - [k^2 - i\omega + ik Pe F(z) \cos \varphi] \hat{\theta} + 2i Ge Pe F'(z) (W'' + k^2 W) \cos \varphi - i Pe A W' \cos \varphi - k Pe^2 G'(z) W = 0, \tag{21b}$$

$$W = 0, \quad W' = 0, \quad \hat{\theta}' = 0 \quad \text{for } z = 0, 1. \tag{21c}$$

We now consider the series expansions

$$W(z) = W_0(z) + W_1(z)k + W_2(z)k^2 + \mathcal{O}(k^3),$$

$$\hat{\theta}(z) = \hat{\theta}_0(z) + \hat{\theta}_1(z)k + \hat{\theta}_2(z)k^2 + \mathcal{O}(k^3),$$

$$Pe = Pe_0 + Pe_1 k + Pe_2 k^2 + \mathcal{O}(k^3),$$

$$\omega = \omega_0 + \omega_1 k + \omega_2 k^2 + \mathcal{O}(k^3), \tag{22}$$

we substitute them into Eqs. (21) and separately solve the differential problems to every order k^n with $n = 0, 1, 2, \dots$. To order k^0 , we just obtain

$$W_0(z) = 0, \quad \hat{\theta}_0(z) = 1, \quad \omega_0 = 0. \tag{23}$$

We note that $\hat{\theta}_0(z)$ could have been set equal to any real or complex constant. In fact, choosing $\hat{\theta}_0(z) = 1$ is just the simplest way to break the scale invariance for the solution of a homogeneous boundary value problem by imposing the constraint $\hat{\theta}(0) = 1$. Hence, for every $n > 0$, one has the extra boundary condition $\hat{\theta}_n(0) = 0$. On account of Eq. (23), the boundary value problem to order k^1 can be written as

$$W_1'''' - 1 = 0, \tag{24a}$$

$$\hat{\theta}_1'' + i [\omega_1 - Pe_0 F(z) \cos \varphi] + 2i Ge Pe_0 F'(z) W_1'' \cos \varphi - i Pe_0 A W_1' \cos \varphi = 0, \tag{24b}$$

$$W_1(0) = 0, \quad W_1'(0) = 0, \quad \hat{\theta}_1(0) = 0, \quad \hat{\theta}_1'(0) = 0,$$

$$W_1(1) = 0, \quad W_1'(1) = 0. \tag{24c}$$

The solution can be easily found though we omit here the expressions of $W_1(z)$ and $\hat{\theta}_1(z)$ for the sake of brevity. We just mention that the boundary condition $\hat{\theta}_1'(1) = 0$ is not needed to determine the unique solution of Eqs. (24), but imposing such an extra condition allows one

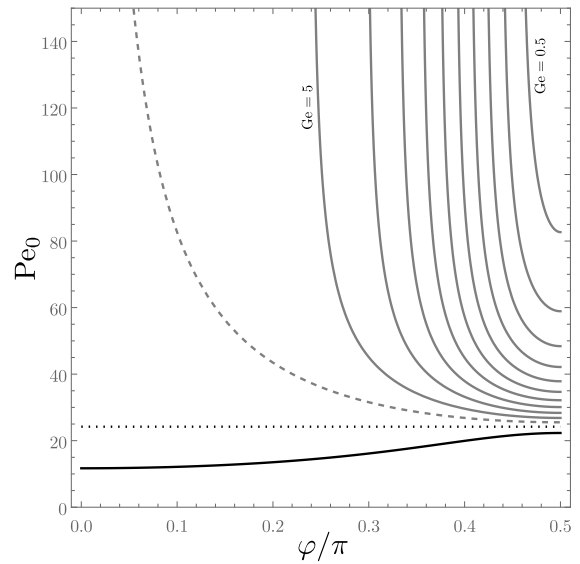


Fig. 6. Plots of Pe_0 versus φ , with $A = A_-$. The solid grey lines are from $Ge = 0.5$ to $Ge = 5$ in steps of 0.5. The dashed line is for $Ge = 5.47464$, the dotted line is for $Ge = 5.99306$ and the solid black line is for $Ge = 3\sqrt{5}$.

to write

$$\omega_1 = \frac{Pe_0 (180 - A Ge) \cos \varphi}{360}, \tag{25}$$

with Pe_0 yet undetermined. On account of Eq. (23), the boundary value problem to order k^2 is given by

$$W_2'''' - \hat{\theta}_1 = 0, \tag{26a}$$

$$\hat{\theta}_2'' - 1 + i\omega_2 - i Pe_1 F(z) \cos \varphi + i [\omega_1 - Pe_0 F(z) \cos \varphi] \hat{\theta}_1 + 2i Ge Pe_1 F'(z) W_1'' \cos \varphi + 2i Ge Pe_0 F'(z) W_2'' \cos \varphi - i Pe_1 A W_1' \cos \varphi - i Pe_0 A W_2' \cos \varphi - Pe_0^2 G'(z) W_1 = 0, \tag{26b}$$

$$W_2(0) = 0, \quad W_2'(0) = 0, \quad \hat{\theta}_2(0) = 0, \quad \hat{\theta}_2'(0) = 0, \\ W_2(1) = 0, \quad W_2'(1) = 0. \tag{26c}$$

Again, we omit the explicit expressions of $W_2(z)$ and $\hat{\theta}_2(z)$ for the unique solution of Eqs. (26). We only stress that the extra boundary condition, $\hat{\theta}_2'(1) = 0$, not involved in the boundary value problem (26) yields an explicit and unique expression for a positive Pe_0 ,

$$Pe_0 = 720 \sqrt{154} \left\{ 2A(A + 66) Ge^2 \cos(2\varphi) - 220[(A - 81)A + 1512] \cos(2\varphi) + 55440(Ge - 6) + A [2(A + 66) Ge^2 + 77A Ge + 220(9 - 2A)] \right\}^{-1/2}. \tag{27}$$

It must be stressed that Pe_0 has a very important physical meaning. As a matter of fact, Pe_0 yields the neutral threshold for linear instability with perturbation normal modes having $k \rightarrow 0$.

Eq. (27), which holds both for $A = A_-$ and $A = A_+$, gives a real positive value of Pe_0 only for values of Ge and φ such that the expression in curly brackets on the right hand side is non-negative. However, this condition does not hold for every possible pair (Ge, φ) .

Fig. 5 shows the domains of existence for Pe_0 , evaluated through Eq. (27), by considering either the branch $A = A_-$ or the branch $A = A_+$. An interesting fact is that, by setting $A = A_-$, Pe_0 exists for longitudinal modes ($\varphi = \pi/2$) within the whole range $0 < Ge \leq 3\sqrt{5}$. For every other value of φ , there is always a minimum Ge below which Pe_0 does not exist. Some plots of Pe_0 versus φ , also relative to the choice $A = A_-$, are reported in Fig. 6 for different values of Ge . In this figure, there are grey lines relative to Ge from 0.5 to 5 in steps of 0.5, while the line of maximum Ge is drawn as a black line. There are also a dotted line and a dashed line corresponding to a couple of special values of

Table 1

Comparison for the A_- branch between the values of Pe_0 , obtained by the analytical expression (27), and the neutral stability value of Pe with $k = 0.1$ computed numerically by the shooting method.

Ge	$Pe_0 (\varphi = \pi/2)$	$Pe (k = 0.1, \varphi = \pi/2)$	$Pe_0 (\varphi = 0)$	$Pe (k = 0.1, \varphi = 0)$
0.1	183.638	183.670	–	–
0.2	130.083	130.106	–	–
0.5	82.6889	82.7033	–	–
0.8	65.6755	65.6869	–	–
1	58.9108	58.9211	–	–
2	42.1479	42.1552	–	–
4	30.1012	30.1061	–	–
6	24.1831	24.1861	24.0109	24.0554
$3\sqrt{5}$	22.3114	22.3123	11.7021	11.7142

Ge. The dotted line, for $Ge = 5.99306$, identifies a special case where Pe_0 is independent of φ and has the value 24.2005. The dashed line is relative to $Ge = 5.47464$, which is the value of Ge bounding from below the range where Pe_0 exists for transverse modes ($\varphi = 0$). From Fig. 6, one may infer that the transverse modes are the most unstable among the modes with infinite wavelength if $5.99306 < Ge \leq 3\sqrt{5}$. A different scenario exists when $0 < Ge < 5.99306$ as the longitudinal modes turn out to be the most unstable.

5. Discussion of the results

The neutral stability condition for the normal modes with infinite wavelength could be found through an analytical solution by employing a power series expansion with respect to the wavenumber k . Extending the scope to perturbation modes with a finite wavelength implies a numerical solution of Eqs. (19).

5.1. Numerical method

The analysis carried out in Section 4.2 highlighted that Eqs. (19) yields an eigenvalue problem. With either $A = A_-$ or $A = A_+$, one may consider (k, φ, Ge) as input parameters and obtain (Pe, ω) as the eigenvalues. The strategy is that defined by the shooting method [31,32]. The first step is setting up a numerical solver for the boundary value problem

$$W'''' - 2k^2 W'' + k^4 W - k^2 \Theta = 0, \tag{28a}$$

$$\Theta'' - [k^2 - i\omega + ikPeF(z)\cos\varphi]\Theta + \frac{2iGePeF'(z)\cos\varphi}{k}(W'' + k^2W) - \frac{iPeA\cos\varphi}{k}W' - Pe^2G'(z)W = 0, \tag{28b}$$

$$W(0) = 0, \quad W'(0) = 0, \quad \Theta(0) = 1, \quad \Theta'(0) = 0, \tag{28c}$$

$$W(1) = 0, \quad W'(1) = 0. \tag{28d}$$

The difference between Eqs. (19) and Eqs. (28) is that, in Eqs. (28), we set $\lambda = -i\omega$, we do not impose the homogeneous boundary condition $\Theta'(1) = 0$, but we enforce the inhomogeneous boundary condition $\Theta(0) = 1$ instead, which is not present in Eqs. (19). The latter inhomogeneous condition is legitimate as Eqs. (19) are scale invariant: if (W, Θ) is a solution, also $(CW, C\Theta)$ is a solution, for every complex constant C . Thus, fixing $\Theta(0) = 1$ means picking up a single non-trivial solution (W, Θ) among an equivalence class of possible solutions. The constant 1 can be replaced by any other complex number without affecting the solution of the eigenvalue problem (19). This argument is just the same as that reported in Section 4.3 with reference to the eigenvalue problem (21). Eqs. (28) can be solved, with $A = A_-$ or $A = A_+$, for every fixed set of parameters $(k, \varphi, Ge, Pe, \omega)$. The numerical solution is accomplished by the software tool *Mathematica* (© Wolfram Research, Inc.) via the built-in function `NDSolve`. Eventually, the condition $\Theta'(1) = 0$ excluded from Eqs. (28), but defining the eigenvalue problem (19), is employed to determine the eigenvalues

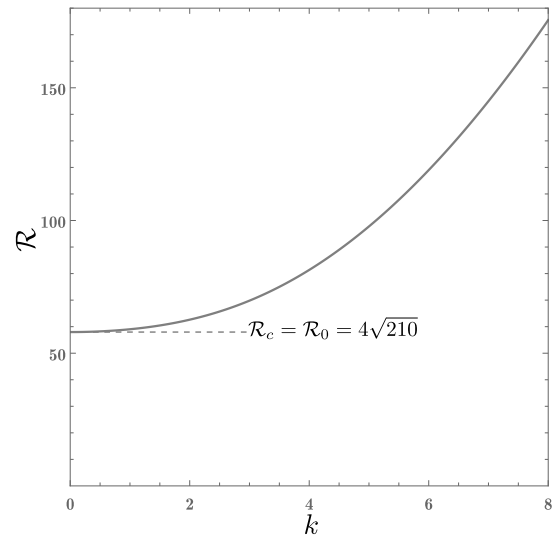


Fig. 7. Neutral stability curve in the (k, \mathcal{R}) plane for longitudinal modes with $A = A_-$ and $Ge \rightarrow 0$.

(Pe, ω) for every input data (k, φ, Ge) . In fact, such a homogeneous condition yields two constraints, $Re[\Theta'(1)] = 0$ and $Im[\Theta'(1)] = 0$, with Re and Im the real and imaginary parts. Thus, this condition leads to the determination of the two real parameters (Pe, ω) . The solution of the target constraints, $Re[\Theta'(1)] = 0$ and $Im[\Theta'(1)] = 0$, is accomplished by using the function `FindRoot` of *Mathematica*. By employing the analytical solution found in Section 4.3, one can initialise the root finding algorithm for the evaluation of (Pe, ω) by starting with $k \rightarrow 0$, for all cases where Pe_0 is defined, and gradually increasing k . Eqs. (22) and (23) imply that, in the limit $k \rightarrow 0$, ω is zero.

By exploring the domain of all possible input parameters (k, φ, Ge) , one may carry out the linear stability analysis. A convenient representation of the results is displayed in the two-dimensional space (k, Pe) , by drawing the neutral stability curve relative to a given pair (φ, Ge) . Graphically, such a curve yields the condition of linear instability as that where Pe exceeds its minimum evaluated along the neutral stability curve. This condition of minimum Pe defines the critical values, (k_c, Pe_c, ω_c) , for the onset of the instability [3,31–33].

A validation of the numerical solver is reported in Table 1 where the data for Pe obtained from the analytical expression (27) are compared with those computed numerically by the shooting method for $k = 0.1$. An excellent agreement is found if one considers that the values of Pe_0 and the neutral stability values of Pe evaluated numerically are relative to slightly different wavenumbers ($k = 0$ and $k = 0.1$). The data for transverse modes with $Ge \leq 4$ are not reported in Table 1 as Pe_0 is undefined when $Ge < 5.47464$ as specified in Section 4.3.

5.2. The regime of small Gebhart number

One can investigate the asymptotic solution of the eigenvalue problem (19) in the limit of small values of Ge . By setting $A = A_-$, one can detect the behaviour at the lowest order in Ge from Eq. (13). Hence, for very small Gebhart numbers, Eqs. (19) can be approximated as

$$W'''' - 2k^2 W'' + k^4 W - k^2 \Theta = 0, \tag{29a}$$

$$\Theta'' - [k^2 - i\omega + ikPe z \cos\varphi]\Theta + \frac{2iGePe \cos\varphi}{k}(W'' + k^2W) - \frac{2iGePe \cos\varphi}{k}W' + GePe^2 z(1-z)W = 0, \tag{29b}$$

$$W = 0, \quad W' = 0, \quad \Theta' = 0 \quad \text{for } z = 0, 1. \tag{29c}$$

The first consideration is that the limit $Ge \rightarrow 0$ can be taken by taking, contextually, also the limit $Pe \rightarrow \infty$ (see the discussion of this point

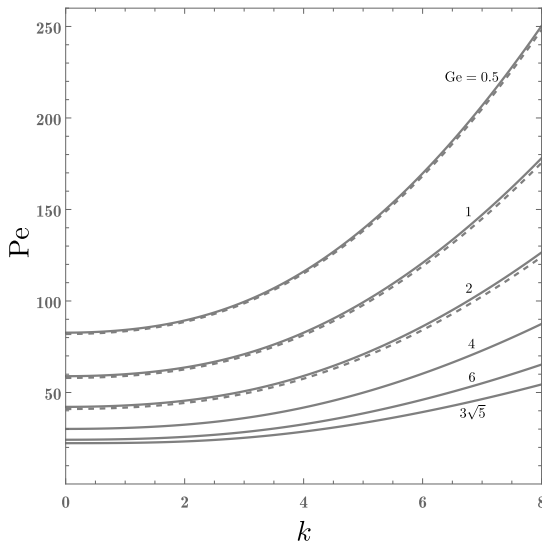


Fig. 8. Neutral stability curves (solid lines) in the (k, Pe) plane for longitudinal modes with $A = A_-$ and Ge ranging from 0.5 to its maximum value $3\sqrt{5}$. The dashed lines display, for $Ge = 0.5, 1$ and 2 , the neutral stability data evaluated with the asymptotic solution for $Ge \ll 1$.

in Barletta et al. [18]). This double limit is well-defined provided that one considers

$$\mathcal{R} = Pe\sqrt{Ge} \sim \mathcal{O}(1). \tag{30}$$

Thus, Eqs. (29) can be rewritten as

$$W'''' - 2k^2 W'' + k^4 W - k^2 \Theta = 0, \tag{31a}$$

$$\Theta'' - \left[k^2 - i\omega + ik \frac{\mathcal{R}}{\sqrt{Ge}} z \cos \varphi \right] \Theta + \frac{2i\sqrt{Ge}\mathcal{R} \cos \varphi}{k} (W'' + k^2 W) - \frac{2i\sqrt{Ge}\mathcal{R} \cos \varphi}{k} W' + \mathcal{R}^2 z(1-z)W = 0, \tag{31b}$$

$$W = 0, \quad W' = 0, \quad \Theta' = 0 \quad \text{for } z = 0, 1. \tag{31c}$$

There are two possible outcomes for the limit $Ge \rightarrow 0$ which depend on the inclination angle φ . If $\cos \varphi \neq 0$ or, equivalently, if $\varphi \neq \pi/2$, the limit $Ge \rightarrow 0$ with $\mathcal{R} \sim \mathcal{O}(1)$ yields a dominant term in Eq. (31b), of order $Ge^{-1/2}$, so that this equation can be satisfied only with $\Theta = 0$. By substituting $\Theta = 0$ in Eq. (31a), the unique solution of Eqs. (31a) and (31c) is $W = 0$. In other words, there are no perturbation modes leading to a neutral stability condition with $\varphi \neq \pi/2$. On the other hand, if $\varphi = \pi/2$, there exists a limiting formulation of Eqs. (31) for $Ge \rightarrow 0$,

$$W'''' - 2k^2 W'' + k^4 W - k^2 \Theta = 0, \tag{32a}$$

$$\Theta'' - (k^2 - i\omega)\Theta + \mathcal{R}^2 z(1-z)W = 0, \tag{32b}$$

$$W = 0, \quad W' = 0, \quad \Theta' = 0 \quad \text{for } z = 0, 1, \tag{32c}$$

which admits non-trivial solutions.

The eigenvalue problem (32) may be solved numerically to determine the neutral stability curve for the longitudinal modes ($\varphi = \pi/2$) in the (k, \mathcal{R}) plane. Such a curve is depicted in Fig. 7. The first comment is that the neutral stability curve represents \mathcal{R} as a monotonic increasing function of k , so that the critical value of \mathcal{R} is

$$\mathcal{R}_c = \mathcal{R}_0 = \lim_{Ge \rightarrow 0} Pe_0 \sqrt{Ge} = 4\sqrt{210} \approx 57.9655, \tag{33}$$

where the limit in Eq. (33) has been evaluated by using Eq. (27). The role of Eq. (33) is compelling as it provides an analytical expression that can be used to approximate the critical value of Pe for the most unstable modes, viz. the longitudinal modes, at small values of the

Gebhart number,

$$Pe_c = Pe_0 \approx 4\sqrt{\frac{210}{Ge}}. \tag{34}$$

Another important feature of the numerical solution of Eqs. (32) is that, along the neutral stability curve, $\omega = 0$. In fact, this result is a characteristic trait of longitudinal modes at both small and large Gebhart numbers.

5.3. The most unstable perturbation modes

The determination of the most unstable modes or, equivalently, the determination of the angle φ that yields the lowest value of Pe_c for a given Gebhart number is a primary step in the stability analysis. In Section 5.2, we have concluded that, for the asymptotic condition $Ge \ll 1$, the longitudinal modes lead the transition to linear instability with Pe_c evaluated analytically through Eq. (34). The oblique or transverse modes, having $\varphi \neq \pi/2$, do not yield any asymptotic condition of neutral stability in this asymptotic case. In practice, such a behaviour means that Pe_c for oblique or transverse modes tends to infinity much faster than for the longitudinal modes when $Ge \rightarrow 0$. Thus, we figure out a scenario where, for small Gebhart numbers, the selected modes at the onset of the linear instability are longitudinal. In particular, the transition is activated by longitudinal modes with infinite wavelength, i.e. $Pe_c = Pe_0$.

As illustrated in Fig. 8, the critical value of Pe for longitudinal modes, relative to $A = A_-$, coincides with Pe_0 whatever is the prescribed Gebhart number. In fact, all the neutral stability curves show Pe as a monotonic increasing function of k . By inspecting Fig. 8, the neutral stability data reported in Fig. 7 for the limiting case $Ge \ll 1$ turn out to determine, through the scaling $Pe = \mathcal{R}/\sqrt{Ge}$, the neutral stability condition with a rough accuracy for $Ge = 2$ (the maximum relative discrepancy is 2.8%), a fair accuracy for $Ge = 1$ (the maximum relative discrepancy is 1.6%) and an even better accuracy for $Ge = 0.5$ (the maximum relative discrepancy is 0.86%). Hence, for practical purposes, the asymptotic solution with $Ge \ll 1$ can be safely employed for all cases with $Ge \leq 0.5$.

As already highlighted in Section 4.3, for infinite wavelength ($k \rightarrow 0$), the longitudinal modes are not the most unstable when extremely large Gebhart numbers are considered and, in particular, when $Ge > 5.99306$. Fig. 9 provides a comparison of longitudinal and transverse modes beyond the quite specific condition $k \rightarrow 0$. This figure suggests that the behaviour conceived for the modes with infinite wavelength indeed holds in general. Indeed, Fig. 9 shows that the lowest minimum of the neutral stability curves for either longitudinal or transverse modes, for a given Gebhart number, is always at $k \rightarrow 0$. This means that the leading critical condition for the onset of the linear instability is that already discussed in Section 4.3. Linear instability is triggered by transverse modes if $5.99306 < Ge \leq 3\sqrt{5}$, while it is started by longitudinal modes if $0 < Ge < 5.99306$. Exploring Gebhart numbers below $Ge = 0.5$ means just widening the gap between the neutral stability curve for longitudinal modes and that for transverse modes. Thus, one recovers the expected trend where the neutral stability threshold for transverse modes tends to an infinite Pe when $Ge \rightarrow 0$ more rapidly than $1/\sqrt{Ge}$, as anticipated with the analysis carried out in Section 5.2.

The intermediate conditions where $0 < \varphi < \pi/2$ can be inspected in an efficient way by tracking the change of Pe versus φ with a given Gebhart number and wavenumber. Fig. 10 displays a major result as it suggests that the transition to linear instability is always driven by the $k = 0$ modes: either transverse at the extremely large Gebhart numbers close to the maximum, $Ge = 3\sqrt{5}$, or longitudinal when the Gebhart number is smaller than the threshold detected in Section 4.3, namely for $Ge < 5.99306$. In fact, we recall that $Ge = 5.99306$ yields the special case where Pe_0 is independent of φ , so that the onset of instability is triggered by any infinite wavelength modes whatever is

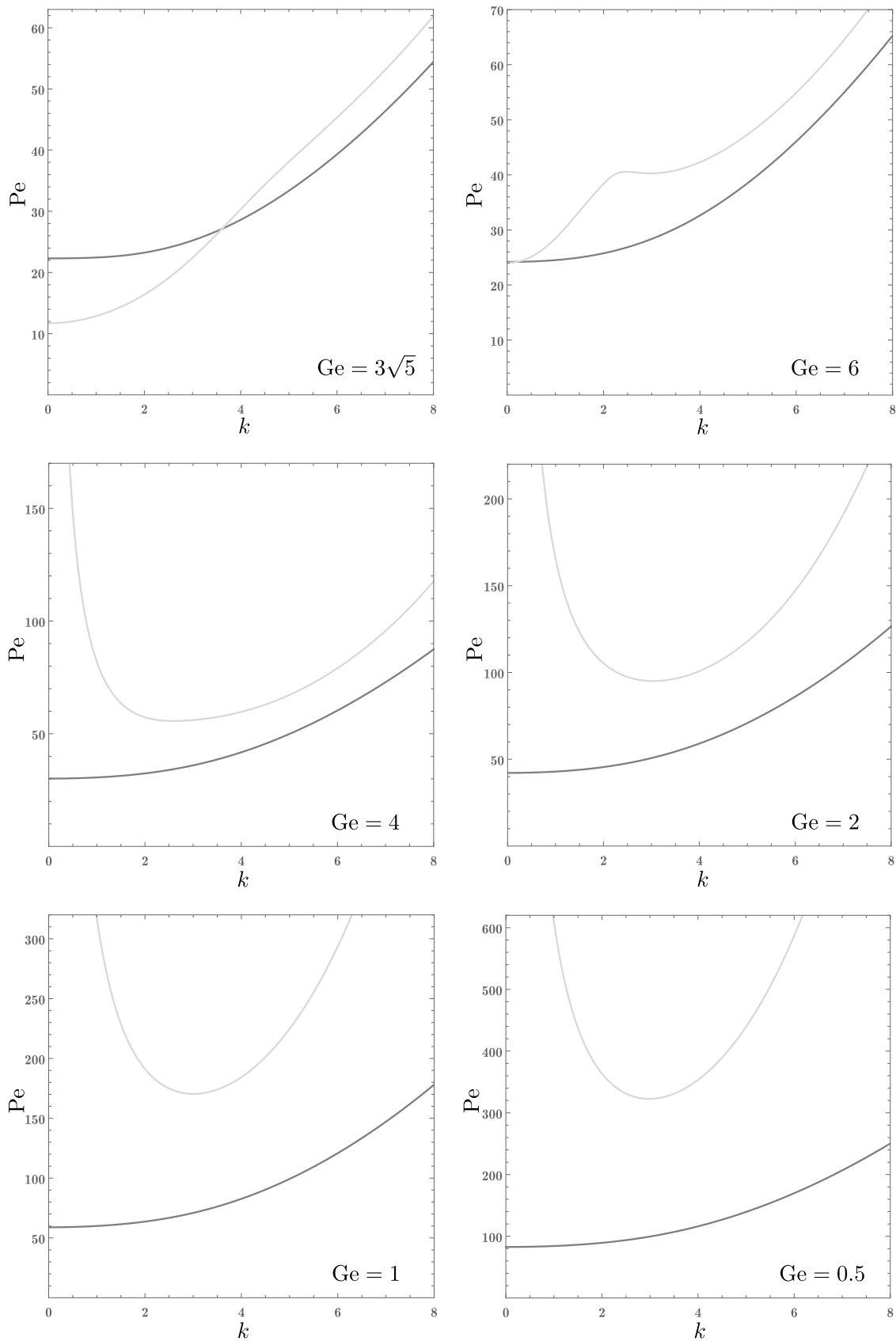


Fig. 9. Neutral stability curves in the (k, Pe) plane with $A = A_-$ for longitudinal modes (dark grey lines) and transverse modes (light grey lines).

their orientation in the horizontal plane. Then, we can take it as a general result that the critical Péclet number, Pe_c , for the initiation

of the instability does always coincide with Pe_0 for either $\varphi = 0$ or $\varphi = \pi/2$ depending on the Gebhart number. Another feature displayed

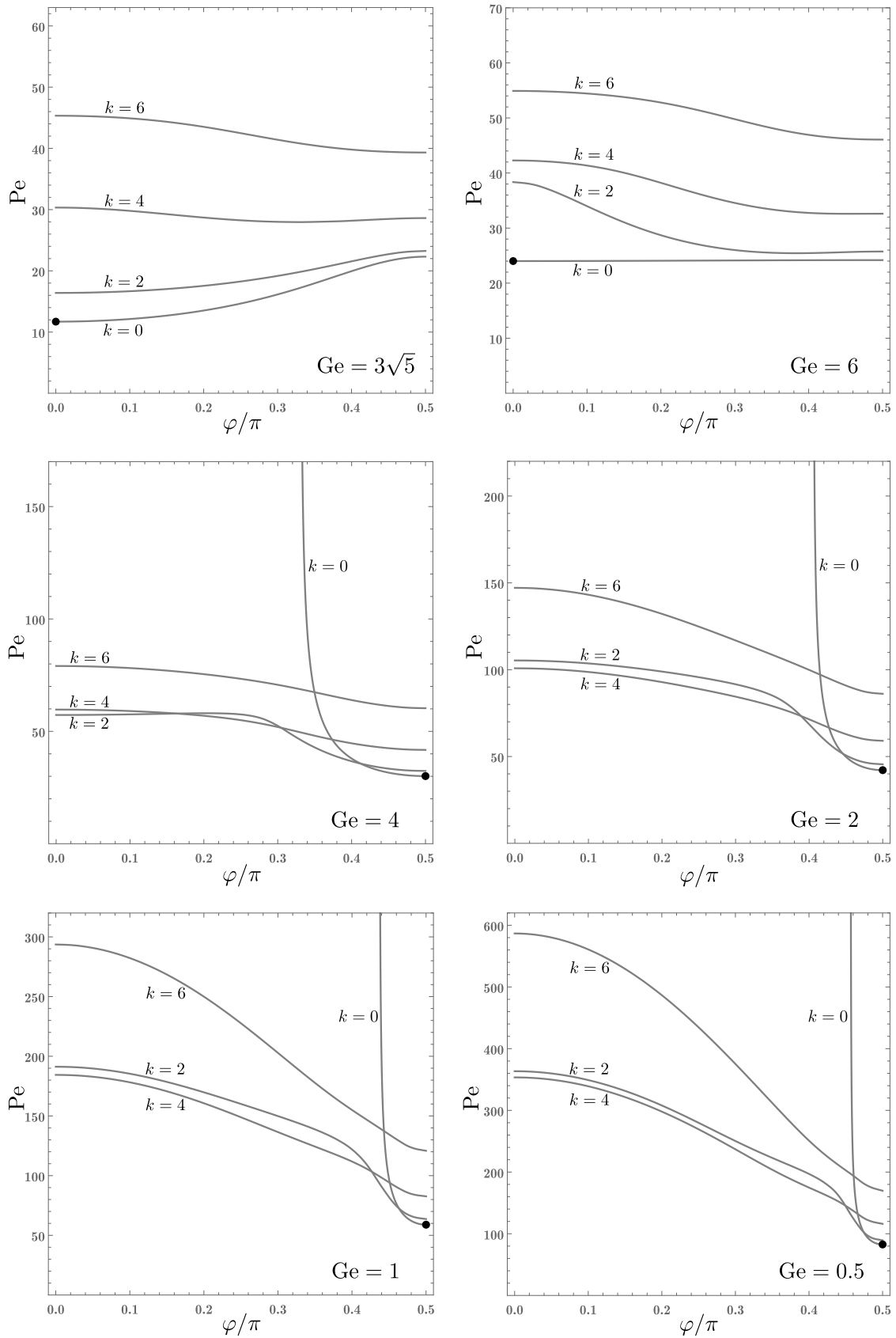


Fig. 10. Neutral stability values of Pe versus φ with $A = A_-$ for oblique modes at different wavenumbers. The black dots denote the minimum values of Pe for the transition to linear instability.

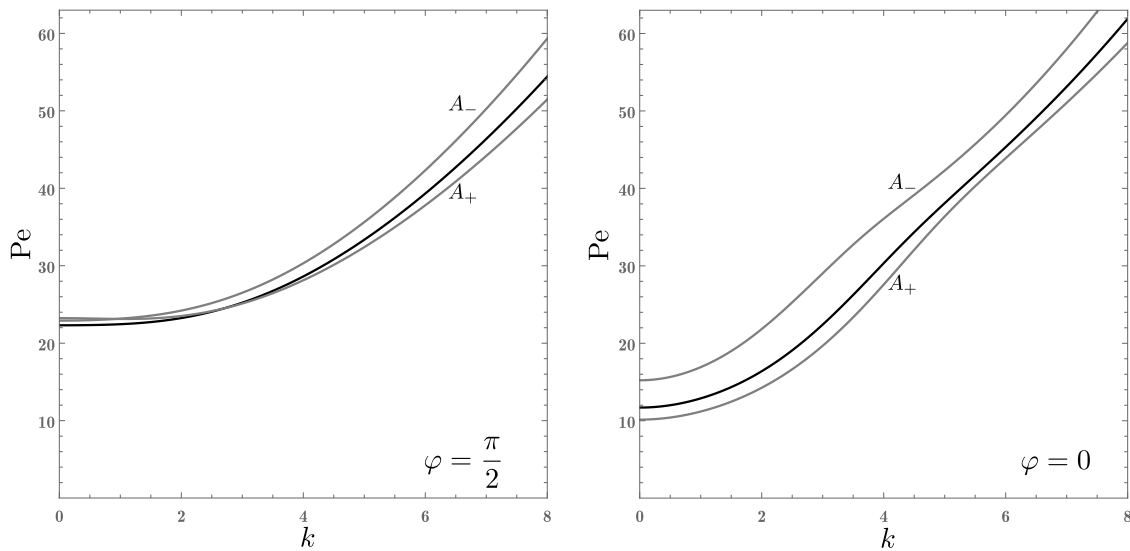


Fig. 11. Neutral stability curves in the (k, Pe) plane for $Ge = 6.5$ (grey lines) and $Ge = 3\sqrt{5}$ (black line) relative to longitudinal modes ($\varphi = \pi/2$) and transverse modes ($\varphi = 0$) with either $A = A_-$ or $A = A_+$.

Table 2

Thermophysical properties of unused engine oil at an average temperature of 300 K [34].

kinematic viscosity, ν [m ² /s]	5.50×10^{-4}
thermal diffusivity, α [m ² /s]	8.53×10^{-8}
specific heat, c [J/(kg K)]	1910
thermal expansion coefficient, β [1/K]	7×10^{-4}
Prandtl number	6450

by Fig. 10 is that the neutral stability value of Pe may depend non-monotonically on φ for a few cases as, for instance $k = 2$ with either $Ge = 4$ or 6.

5.4. Close to the maximum Gebhart number

We have stressed that the maximum possible Gebhart number, $3\sqrt{5}$, is an extremely large value for most common applications, possibly also at large spatial scales such as those pertaining to geophysical systems. This said, it may be a matter of completeness in the stability analysis considering also the comparison between cases on the A_- branch and the A_+ branch envisaged in Fig. 4. An illustration of the transition to linear instability close to $Ge = 3\sqrt{5}$ is displayed in Fig. 11. Besides the expected similarity of the neutral stability curves for $A = A_-$ and $A = A_+$, an important result is that the transition to instability is driven by transverse modes with an infinite wavelength. Furthermore, the branch $A = A_+$ turns out to be more unstable than the branch $A = A_-$. Longitudinal modes are not involved in the initiation of the instability and they show up an uneven behaviour on comparing the two branches $A = A_-$ and $A = A_+$. In fact, the branch $A = A_+$ of longitudinal modes shows up a minimum condition for the Péclet number $Pe_c = 23.1290$ with $k_c = 1.07691$. Among the cases reported in Fig. 11, the latter is the only one where the neutral stability curve involves a Péclet number not monotonically increasing with k .

5.5. A thought experiment

The analysis carried out so far is entirely based on dimensionless quantities, but it may be interesting to check for possible applications or even conceivable experimental validations of the results in some specific cases.

We assumed from the beginning of the stability analysis that the fluid is to be considered as extremely viscous and with a low thermal

diffusivity so that its Prandtl number can reasonably be considered as very large, consistently with the creeping flow assumption. An example can be an unused engine oil whose properties at an average temperature of 300 K are reported in Table 2. Let us assume that a Couette experimental setup is designed with a distance $H = 1$ cm between the walls in relative motion. Then, by employing the data reported in Table 2, the Gebhart number turns out to be extremely small,

$$Ge = 3.60 \times 10^{-8}. \quad (35)$$

With such a small Gebhart number, the basic velocity profile is practically indistinguishable from the isothermal linear profile for the Couette flow. Furthermore, we can consistently employ Eq. (34), deduced for $Ge \ll 1$, in order to evaluate the critical Péclet number leading to the linear instability of the basic flow,

$$Pe_c = Pe_0 \approx 4 \sqrt{\frac{210}{Ge}} = 306\,000. \quad (36)$$

As the transition to instability predicted by our study occurs by longitudinal perturbation modes with infinite wavelength superposed to the basic flow, the qualitative overall flow pattern changes from the straight parallel streamlines of the basic flow to the mutually oblique straight streamlines of the perturbed flow. We might also recall that, as the transition to instability occurs by the longitudinal modes ($\varphi = \pi/2$), the streamwise direction of the basic flow is the y axis.

Finally, by employing Table 2, one can determine the critical Reynolds number for the linear instability of the Couette flow,

$$Re_c = \frac{Pe_c}{Pr} = 47.4. \quad (37)$$

Interestingly enough, this small critical Reynolds number might be compared with those obtained for the isothermal Couette flow on evaluating the threshold for the nonlinear hydrodynamic stability via the energy method [35–37].

Let us employ the definition of the dimensional scale for the temperature, Eq. (4), and the expression of the dimensionless temperature distribution in the basic state given by Eqs. (9)–(11). Then, one may estimate that, with $Ge = 3.60 \times 10^{-8}$, $Pe = Pe_c = 306\,000$ and $A = A_-$, the temperature gap between the lower and the upper wall at a given streamwise cross-section, $y = \text{constant}$, is 3.8 K. Moreover, the streamwise basic temperature gradient, 1.5×10^{-4} K/m, is definitely negligible. Over such a temperature range, the standard formulation

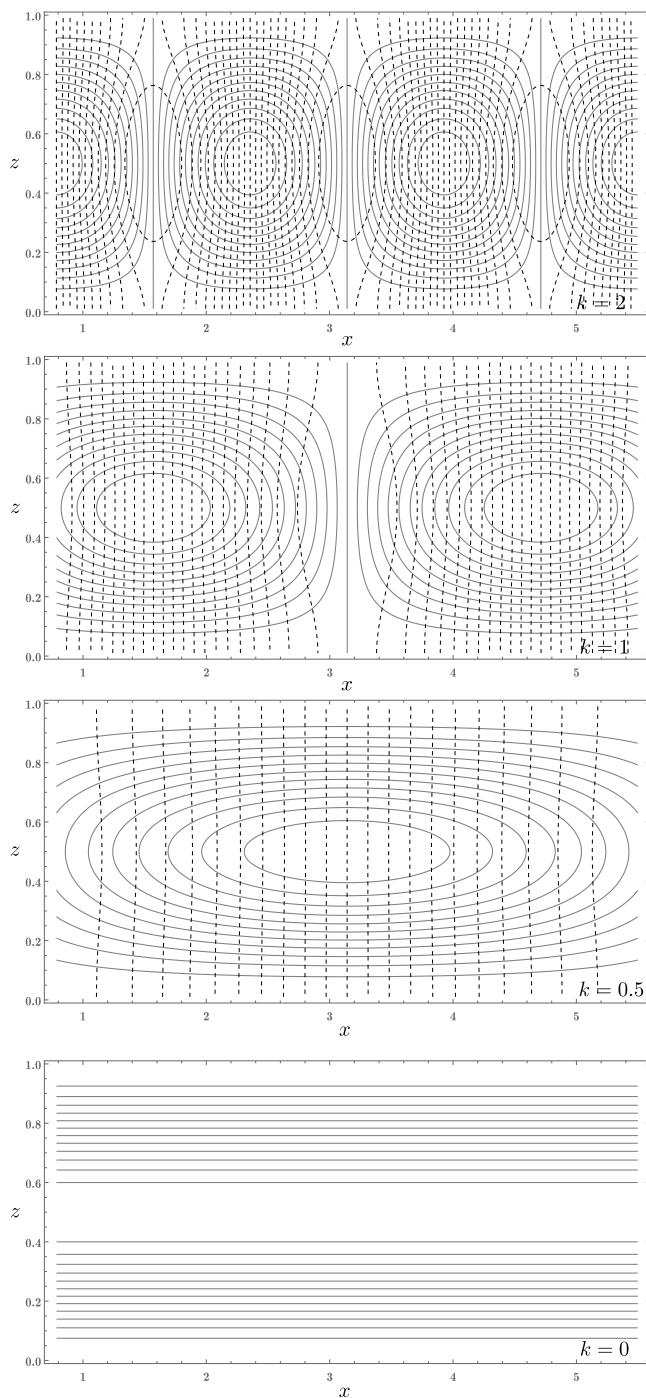


Fig. 12. Streamlines (solid) and isotherms (dashed) for the secondary flow obtained for decreasing wavenumbers $k = 2, 1, 0.5, 0$ with parametric values along the neutral stability curve, Fig. 7, relative to the asymptotic regime of small Ge described in Section 5.2.

of the problem based on the Oberbeck–Boussinesq approximation may be considered as consistent.

5.6. Further physical considerations

The onset of thermal instability examined in our analysis is caused by the interplay between the viscous dissipation effect and the buoyancy force modelled within the Boussinesq approximation. The viscous dissipation, or frictional heating, is the source of a basic stationary

temperature gradient with both a nonzero streamwise component and a nonzero vertical component. The buoyancy force then is the cause of the secondary flow for the transition to instability.

In order to illustrate the features of such a secondary flow, we consider the asymptotic case of a small Gebhart number discussed in Section 5.2. In particular, as $k_c = 0$, we show the streamlines and the isotherms for three decreasing values of k along the neutral stability curve displayed in Fig. 7. As k decreases, the horizontal width of the convection cells becomes larger and larger tending to infinity when $k \rightarrow k_c = 0$. In this limit, the streamlines of the secondary flow tend to become horizontal straight lines. In fact, Fig. 12 illustrates the change of the cellular patterns associated with decreasing wavenumbers $k = 2, k = 1, k = 0.5$ and $k = 0$ for neutral stability conditions corresponding to the small- Ge asymptotic solution. As expected, the streamlines for the case $k = 0$ are straight lines, thus depicting an infinite width convection cell. No isotherms are drawn in the frame for $k = 0$. In fact, as suggested by the frame for $k = 0.5$, when k decreases, the secondary flow tends to display approximately vertical isotherms. This behaviour implies that the secondary flow temperature depends almost only on the horizontal coordinate x through the e^{ikx} factor, as shown by Eq. (16). Such a factor tends to 1 in the limit $k \rightarrow 0$ and, hence, also the dependence on x is lost.

6. Conclusions

The stationary parallel flows in a horizontal plane channel with adiabatic rigid walls have been studied. The viscous dissipation effect caused by the imposed relative velocity between the boundary walls has been taken into account in the local energy balance. The flow description adopted and, in particular, the temperature coupling in the local momentum balance has been modelled according to the Oberbeck–Boussinesq approximation. As a result, the basic flows turned out to be non-isothermal displaying Couette-like velocity profiles. It has been shown that there exist dual flow branches corresponding to given values of the Péclet number, Pe , and of the Gebhart number, Ge . The dual flows coincide when $Ge = 3\sqrt{5}$. No stationary parallel flows exist when $Ge > 3\sqrt{5}$. It has been pointed out that only one of these dual flow branches, denoted as the A_- branch, is compatible with the Oberbeck–Boussinesq approximation for realistic, *i.e.* sufficiently small, Gebhart numbers.

A linear stability analysis focussed on the A_- branch has been carried out in a creeping flow regime where the Prandtl number has been considered infinite. Arbitrarily oriented wavelike perturbations have been regarded, ranging from the longitudinal modes propagating in a direction perpendicular to the basic flow direction to the transverse modes, whose direction of propagation is parallel to the basic flow direction. All intermediate inclinations, namely the oblique modes, have been also considered. The main conclusions drawn from such an analysis can be outlined as follows:

- A numerical solution of the stability eigenvalue problem has been obtained, based on the shooting method. The objective has been the determination of the neutral stability curves in the (k, Pe) plane. Hence, it has been shown that, in every case, the smallest neutrally stable Péclet number, *i.e.* the critical value of Pe , corresponds to the limit $k \rightarrow 0$ (infinite wavelength).
- The initiation of the instability occurs when the Péclet number becomes larger than its critical value, which depends on the Gebhart number. The most unstable perturbation modes have an infinite wavelength. They are either longitudinal modes, for $Ge < 5.99306$, or transverse modes, for $5.99306 < Ge \leq 3\sqrt{5}$. The case $Ge = 5.99306$ is special as the transition to instability is independent of the mode orientation, *i.e.* longitudinal, oblique and transverse modes are equivalent.
- An analytical solution of the stability eigenvalue problem has been obtained for the asymptotic case where the wavenumber, k ,

is vanishingly small and, as a consequence, the wavelength tends to infinity. Thus, in every case, the determination of the critical Péclet number is analytical.

- The regime of small Gebhart numbers has been explored by an asymptotic solution. This regime is typical of flows on a laboratory scale, while cases where the Gebhart number is of the order of unity can only be pertinent for the study of geophysical or astrophysical systems [28,38]. As for the analogous case of Poiseuille-like flows [18], the $Ge \ll 1$ asymptotic solution reveals that the neutral stability Péclet number for longitudinal modes scales with $Ge^{-1/2}$. As expected from the proof by Romanov [2], the basic flows turn out to be stable at any Péclet number when $Ge \rightarrow 0$.
- Based on the $Ge \ll 1$ asymptotic solution, an experimental setup has been proposed for a possible validation of the results relative to flows having a vertical width compatible with the size of a laboratory equipment.

There are several opportunities for future developments of the results obtained in this paper. The extension of the classical Oberbeck–Boussinesq approximation for convective flows to cases where the fluid viscosity undergoes a sensible temperature change may be important. Another possible improvement in the model adopted is relaxing the assumption of creeping flow for the perturbation dynamics or, equivalently, extending the study to cases with a finite Prandtl number. The nonlinearity of the transition to instability is another important issue. Its analysis could disclose the emergence of a possible subcritical instability and provide an effective comparison with the energy method results for the hydrodynamic stability threshold.

Declaration of competing interest

The authors declare that they have no known competing financial interests or personal relationships that could have appeared to influence the work reported in this paper.

Data availability

No data was used for the research described in the article.

Acknowledgements

The authors acknowledge financial support from Italian Ministry of Education, University and Research (MIUR) grant number PRIN 2017F7KZWS.

Appendix. An alternative formulation of the stability analysis

The analysis showing that the basic flow expressed by Eq. (9) leads to the perturbation governing Eqs. (17) can be reformulated by assuming that the basic flow is directed along the x axis and that the general perturbation mode has a wave vector $(k_x, k_y, 0)$ inclined to the x axis.

In order to prove this statement, we start by replacing Eq. (6) with

$$\begin{aligned} \mathbf{u} = 0, \quad \frac{\partial T}{\partial z} = 0 \quad \text{for } z = 0, \\ u = \text{Pe}, \quad v = 0, \quad w = 0, \quad \frac{\partial T}{\partial z} = 0 \quad \text{for } z = 1. \end{aligned} \tag{A.1}$$

Accordingly, we need to rewrite Eq. (9) as

$$\begin{aligned} u_b = \text{Pe } F(z), \quad v_b = 0, \quad T_b = \text{Pe } A x + \text{Pe}^2 G(z), \\ \nabla p_b = \left(\text{Pe } F''(z), 0, T_b \right). \end{aligned} \tag{A.2}$$

We modify Eq. (16) by introducing the wave vector $(k_x, k_y, 0)$,

$$\begin{pmatrix} \mathbf{u} \\ p \\ T \end{pmatrix} = \begin{pmatrix} \mathbf{u}_b \\ p_b \\ T_b \end{pmatrix} + \varepsilon \begin{pmatrix} \tilde{U}(z) \\ P(z) \\ \Theta(z) \end{pmatrix} e^{i(k_x x + k_y y)} e^{\lambda t}, \tag{A.3}$$

with $\tilde{\mathbf{U}} = (\tilde{U}, \tilde{V}, \tilde{W})$. Then, Eqs. (17) are to be replaced by

$$\tilde{W}' + i(k_x \tilde{U} + k_y \tilde{V}) = 0, \tag{A.4a}$$

$$\frac{1}{\text{Pr}} [\lambda \tilde{U} + ik_x \text{Pe } F(z) \tilde{U} + \text{Pe } F'(z) \tilde{W}] = -ik_x P + \tilde{U}'' - k^2 \tilde{U}, \tag{A.4b}$$

$$\frac{1}{\text{Pr}} [\lambda \tilde{V} + ik_x \text{Pe } F(z) \tilde{V}] = -ik_y P + \tilde{V}'' - k^2 \tilde{V}, \tag{A.4c}$$

$$\frac{1}{\text{Pr}} [\lambda \tilde{W} + ik_x \text{Pe } F(z) \tilde{W}] = -P' + \Theta + \tilde{W}'' - k^2 \tilde{W}, \tag{A.4d}$$

$$\begin{aligned} \lambda \Theta + ik_x \text{Pe } F(z) \Theta + \text{Pe } A \tilde{U} + \text{Pe}^2 G'(z) \tilde{W} \\ = \Theta'' - k^2 \Theta + 2 \text{Ge } \text{Pe } F'(z) (\tilde{U}' + ik_x \tilde{W}), \end{aligned} \tag{A.4e}$$

where $k^2 = k_x^2 + k_y^2$. We now define functions $U(z)$, $V(z)$ and $W(z)$ so that

$$k U = k_x \tilde{U} + k_y \tilde{V}, \quad k V = k_y \tilde{U} - k_x \tilde{V}, \quad W = \tilde{W}. \tag{A.5}$$

We can now rewrite Eqs. (A.4) by substituting Eq. (A.5) into Eq. (A.4a), into the combination of k_x times Eq. (A.4b) plus k_y times Eq. (A.4c), into the combination of k_y times Eq. (A.4b) minus k_x times Eq. (A.4c), into Eq. (A.4d) and into k times Eq. (A.4e). The resulting system of differential equations is

$$W' + ik U = 0, \tag{A.6a}$$

$$\begin{aligned} \frac{1}{\text{Pr}} [\lambda k U + ik_x k \text{Pe } F(z) U + k_x \text{Pe } F'(z) W] \\ = -ik^2 P + k U'' - k^3 U, \end{aligned} \tag{A.6b}$$

$$\frac{1}{\text{Pr}} [\lambda k V + ik_x k \text{Pe } F(z) V + k_y \text{Pe } F'(z) W] = k V'' - k^3 V, \tag{A.6c}$$

$$\frac{1}{\text{Pr}} [\lambda W + ik_x \text{Pe } F(z) W] = -P' + \Theta + W'' - k^2 W, \tag{A.6d}$$

$$\begin{aligned} \lambda k \Theta + ik_x k \text{Pe } F(z) \Theta + \text{Pe } A (k_x U + k_y V) + k \text{Pe}^2 G'(z) W \\ = k \Theta'' - k^3 \Theta + 2 \text{Ge } \text{Pe } F'(z) (k_x U' + k_y V' + ik_x k W). \end{aligned} \tag{A.6e}$$

Let us define the inclination angle φ as

$$k_x = k \cos \varphi, \quad k_y = k \sin \varphi. \tag{A.7}$$

We substitute Eq. (A.7) into Eqs. (A.6). Then, we divide Eqs. (A.6b), (A.6c) and (A.6e) by k and we finally obtain Eqs. (17). We conclude that the formulation based on Eqs. (A.1)–(A.3) is completely equivalent to that employed in Sections 2–4 as it leads to the same eigenvalue problem for the stability analysis.

References

- [1] Lord Rayleigh, Further remarks on the stability of viscous fluid motion, London Edinb. Dublin Philos. Mag. J. Sci. 28 (1914) 609–619.
- [2] V.A. Romanov, Stability of plane-parallel Couette flow, Funct. Anal. Appl. 7 (1973) 137–146.
- [3] P.G. Drazin, W.H. Reid, Hydrodynamic Stability, second ed., Cambridge University Press, 2004.
- [4] P.J. Schmid, D.S. Henningson, Stability and Transition in Shear Flows, Springer, 2001.
- [5] S. Bottin, O. Dauchot, F. Daviaud, P. Manneville, Experimental evidence of streamwise vortices as finite amplitude solutions in transitional plane Couette flow, Phys. Fluids 10 (1998) 2597–2607.
- [6] N. Tillmark, P.H. Alfredsson, Experiments on transition in plane Couette flow, J. Fluid Mech. 235 (1992) 89–102.
- [7] A.P. Ingersoll, Convective instabilities in plane Couette flow, Phys. Fluids 9 (4) (1966) 682–689.
- [8] R. Kimura, H. Tsu, A. Yagihashi, Convective patterns in a plane Couette flow, J. Meteorol. Soc. Japan. Ser. II 49 (1971) 249–260.
- [9] R.E. Kelly, The onset and development of thermal convection in fully developed shear flows, in: J.W. Hutchinson, T.Y. Wu (Eds.), Advances in Applied Mechanics, Vol. 31, Elsevier, 1994, pp. 35–112.
- [10] D.D. Joseph, Variable viscosity effects on the flow and stability of flow in channels and pipes, Phys. Fluids 7 (1964) 1761–1771.
- [11] D.D. Joseph, Stability of frictionally-heated flow, Phys. Fluids 8 (1965) 2195–2200.
- [12] A. Barletta, D.A. Nield, Variable viscosity effects on the dissipation instability in a porous layer with horizontal throughflow, Phys. Fluids 24 (2012) 104102.

- [13] J.M. White, S.J. Muller, Experimental studies on the stability of Newtonian Taylor–Couette flow in the presence of viscous heating, *J. Fluid Mech.* 462 (2002) 133–159.
- [14] A. Barletta, D.A. Nield, Convection-dissipation instability in the horizontal plane Couette flow of a highly viscous fluid, *J. Fluid Mech.* 662 (2010) 475–492.
- [15] A. Barletta, M. Celli, D.A. Nield, On the onset of dissipation thermal instability for the poiseuille flow of a highly viscous fluid in a horizontal channel, *J. Fluid Mech.* 681 (2011) 499–514.
- [16] A. Barletta, On the thermal instability induced by viscous dissipation, *Int. J. Therm. Sci.* 88 (2015) 238–247.
- [17] Y. Requilé, S.C. Hirata, M.N. Ouarzazi, Viscous dissipation effects on the linear stability of Rayleigh–Bénard–Poiseuille/Couette convection, *Int. J. Heat Mass Transfer* 146 (2020) 118834.
- [18] A. Barletta, M. Celli, D.A.S. Rees, Viscous heating and instability of the adiabatic buoyant flows in a horizontal channel, *Phys. Fluids* 35 (2023) 033111.
- [19] F. Capone, M. Gentile, Nonlinear stability analysis of convection for fluids with exponentially temperature-dependent viscosity, *Acta Mech.* 107 (1994) 53–64.
- [20] F. Capone, M. Gentile, Nonlinear stability analysis of the Bénard problem for fluids with a convex nonincreasing temperature depending viscosity, *Contin. Mech. Thermodyn.* 7 (1995) 297–309.
- [21] L. Fusi, L. Vergori, The Rayleigh–Bénard problem for a fluid with pressure- and temperature-dependent material properties, *Z. Angew. Math. Phys.* 74 (2023) 8.
- [22] M. Singh, R. Ragoju, G. Shiva Kumar Reddy, C. Subramani, Predicting the effect of inertia, rotation, and magnetic field on the onset of convection in a bidisperse porous medium using machine learning techniques, *Phys. Fluids* 35 (2023) 034103.
- [23] M.T. Horsch, S. Chiacchiera, Y. Bami, G.J. Schmitz, G. Moggi, G. Goldbeck, E. Ghedini, Reliable and interoperable computational molecular engineering: 2, in: *Semantic Interoperability Based on the European Materials and Modelling Ontology*, 2020, arXiv preprint arXiv:2001.04175.
- [24] K.R. Rajagopal, M. Ruzicka, A.R. Srinivasa, On the Oberbeck–Boussinesq approximation, *Math. Models Methods Appl. Sci.* 6 (1996) 1157–1167.
- [25] A. Barletta, The Boussinesq approximation for buoyant flows, *Mech. Res. Commun.* 124 (2022) 103939.
- [26] A. Barletta, M. Celli, D.A.S. Rees, On the use and misuse of the Oberbeck–Boussinesq approximation, *Physics* 5 (2023) 298–309.
- [27] B.A. Davis, P.J. Gramann, M.D.P. Noriega E., T.A. Osswald, Grooved feed single screw extruders—improving productivity and reducing viscous heating effects, *Polym. Eng. Sci.* 38 (1998) 1199–1204.
- [28] C. Kincaid, P. Silver, The role of viscous dissipation in the orogenic process, *Earth Planet. Sci. Lett.* 142 (1996) 271–288.
- [29] A.P. van den Berg, D.A. Yuen, The role of shear heating in lubricating mantle flow, *Earth Planet. Sci. Lett.* 151 (1997) 33–42.
- [30] A. Barletta, M. Celli, P.V. Brandão, On mixed convection in a horizontal channel, viscous dissipation and flow duality, *Fluids* 7 (5) (2022) 170.
- [31] B. Straughan, *The Energy Method, Stability, and Nonlinear Convection*, Springer, 2013.
- [32] A. Barletta, *Routes to Absolute Instability in Porous Media*, Springer, 2019.
- [33] P.K. Kundu, I.M. Cohen, D.R. Dowling, *Fluid Mechanics*, sixth ed., Academic Press, 2016.
- [34] A. Bejan, *Convection Heat Transfer*, third ed., John Wiley & Sons, 2004.
- [35] P. Falsaperla, A. Giacobbe, G. Mulone, Nonlinear stability results for plane Couette and Poiseuille flows, *Phys. Rev. E* 100 (2019) 013113.
- [36] P. Falsaperla, G. Mulone, C. Perrone, Energy stability of plane Couette and Poiseuille flows: A conjecture, *Eur. J. Mech. B Fluids* 93 (2022) 93–100.
- [37] A. Giacobbe, G. Mulone, C. Perrone, Monotonic energy stability for inclined laminar flows, *Mech. Res. Commun.* 125 (2022) 103987.
- [38] T. Miyagoshi, C. Tachinami, M. Kameyama, M. Ogawa, On the vigor of mantle convection in super-Earths, *Astrophys. J. Lett.* 780 (2013) L8.